Scripta Materialia 112 (2016) 15–18

Contents lists available at ScienceDirect

Scripta Materialia

journal homepage: www.elsevier.com/locate/scriptamat

# Role of oxygen atoms in α″ martensite of Ti-20 at.% Nb alloy

Masaki Tahara [a,*], Tomonari Inamura [a], Hee Young Kim [b], Shuichi Miyazaki [b,c], Hideki Hosoda [a]

[a] Precision and Intelligence Laboratory, Tokyo Institute of Technology, 4259 Nagatsutacho, Midori-ku, Yokohama, Kanagawa 226-8503, Japan
[b] Division of Materials Science, University of Tsukuba, 1-1-1 Tennodai, Tsukuba, Ibaraki 305-8573, Japan
[c] Foundation for Advancement of International Science, 3-24-16 Kasuga, Tsukuba, Ibaraki 305-0821, Japan

ARTICLE INFO

*Article history:*
Received 20 May 2015
Accepted 31 August 2015
Available online 18 September 2015

*Keywords:*
Martensitic phase transformation
Titanium alloys
Interstitials
Nanodomains

ABSTRACT

The role of oxygen atoms in the α″ martensite phase was investigated in the Ti-20 at.% Nb alloy by X-ray diffractometry and differential scanning calorimetry. The axial ratio *b*/*a* of α″ martensite and reverse martensitic transformation temperature increased with increasing oxygen content. These results imply that the α″ martensite was stabilized by oxygen atoms, owing to the relaxation of the strain field introduced by the oxygen atoms.

© 2015 Acta Materialia Inc. Published by Elsevier Ltd. All rights reserved.

Ni-free Ti-based shape memory alloys have been widely investigated [1–6]. The shape memory effect and superelasticity of β-type Ti-based alloys arise due to the martensitic transformation from the parent β phase (bcc) to the α″ martensite phase (orthorhombic), and its reverse transformation. The martensitic transformation of Ti-based alloys is a bcc–hcp type transformation, and can be divided into two processes: (1) shuffling of parallel adjacent $\{1\,1\,0\}_\beta$ planes in the $\langle 1\,1\,0 \rangle_\beta$ direction and (2) shearing on the $\{1\,1\,2\}_\beta$ planes in the $\langle 1\,1\,1 \rangle_\beta$ direction. The crystal structure of α″ martensite is intermediate between the bcc (β phase) and hcp (α′ phase). In contrast, the shape memory properties and martensitic transformation behavior of Ti-based shape memory alloys are extremely sensitive to interstitial impurities such as oxygen [4,7–9] and nitrogen [6,10,11]. The addition of oxygen and nitrogen increases the recovery strain owing to the increase in the critical stress for slip caused by the solid-solution hardening. The martensitic transformation start temperature ($M_s$) sharply decreases with the addition of oxygen and nitrogen. The addition of 1 at.% oxygen and nitrogen to the Ti–Nb alloys decreases $M_s$ by 160 and 200 K, respectively. Suppression of the martensitic transformation by the addition of interstitial atoms has been widely confirmed in β-Ti alloys, and its mechanism has been extensively investigated. Hammond [12] suggested that the interstitial atoms that occupy the random octahedral sites of β-Ti alloy inhibit contraction along the *a*-axis of α″ martensite, and $M_s$ decreases with the addition of interstitial atoms. Recently, we reported that randomly distributed oxygen atoms and their local strain fields generate nanosized local lattice modulations (nanodomains) in the parent β phase, and these nanodomains play a key role in the β–α″ martensitic transformation of Ti–Nb alloys [13–15]. Nanodomains suppress the long-range martensitic transformation from the parent β phase to the α″ martensite phase, and cause unique phenomena such as non-linear elastic deformation [16], invar-like behavior [15], and heating-induced forward martensitic transformation [17]. Previous studies of the effect of oxygen atoms on the martensitic transformation of β-Ti alloys were performed for the oxygen atoms in parent β phase. However, the role of oxygen atoms in the α″ martensite remains to be clarified. In this study, we investigated the effect of oxygen addition on the crystal structure and phase stability of α″ martensite in Ti–Nb alloys by X-ray diffraction (XRD) and differential scanning calorimeter (DSC). The relationship between the oxygen atoms and the phase stability of α″ martensite was discussed based on the interstitial sites of the oxygen atoms in α″ martensite.

The (Ti-20Nb)-(0, 0.3, 0.5, 0.7, and 1.0)O (at.%) ingots were prepared by Ar arc melting and homogenized at 1273 K for 7.2 ks in an Ar atmosphere, followed by water quenching. These alloys are denoted by their oxygen content (0O, 0.3O, 0.5O, 0.7O, and 1.0O). The ingots were cold-rolled to a reduction in thickness of 98%. An electrical discharge machine was used to cut specimens for XRD and DSC measurements. The specimens were mechanically polished and chemically etched to remove surface damage. The specimens were solution-treated at 1173 K for 1.8 ks in an Ar atmosphere, followed by water quenching. The oxidized surface was removed by chemical etching, and XRD measurements were carried out with Cu Kα radiation at room temperature. Silicon powder was used as reference material in XRD measurements. DSC measurements were conducted at a controlled heating rate of 10 K/min.

* Corresponding author.
*E-mail address:* tahara.m.aa@m.titech.ac.jp (M. Tahara).

http://dx.doi.org/10.1016/j.scriptamat.2015.08.033
1359-6462/© 2015 Acta Materialia Inc. Published by Elsevier Ltd. All rights reserved.

Fig. 1 shows the XRD profiles of the 0O, 0.3O, 0.5O, 0.7O, and 1.0O alloys. Only the α″ martensite phase was observed in the 0O alloy, whereas the α″ martensite and β parent phases were observed in the 0.3O alloy. The peak intensity of the β phase increased as the oxygen content was increased from 0.3 to 0.5 at.%. This implies that the oxygen addition lowers the martensitic transformation finish temperature ($M_f$) to below room temperature, which is consistent with previous reports [4,7,9,12]. In the 0.7O and 1.0O alloys, the α″ martensite phase was not observed, meaning that the $M_s$ points of these two alloys were below room temperature. Oxygen atoms in the parent β phase generate nanodomains, which suppress the β–α″ martensitic transformation [13,14]. Therefore, long-range α″ martensite was not formed in the alloys with higher oxygen contents. Reflection peaks from the athermal-ω phase were also observed in the oxygen-added alloys, and the peak intensities of the athermal-ω phase were increased by increasing the oxygen content from 0.3 to 0.7 at.%. These changes in the XRD profile are due to the fact that the volume fraction of the parent β phase increases by the oxygen addition and the athermal-ω phase is formed only in the parent β phase. As the oxygen content increased from 0.7 to 1.0 at.%, the peak intensity of the athermal-ω phase decreased. These observations show that the addition of oxygen suppresses the formation of the athermal-ω phase, and similar results were reported in Ti–V alloys by Paton and Williams [18].

Lattice constants of α″ martensite in the 0O, 0.3O, and 0.5O alloys were determined by the XRD profiles and the results are shown in Fig. 2(a). The *a*-axis of α″ martensite decreased with increasing oxygen content, whereas the *b*- and *c*-axes of α″ martensite increased. The unit-cell volume of the α″ martensite linearly increased with increasing oxygen content (Fig. 2(b)). These results imply that the oxygen atoms dissolved in the α″ martensite and occupied the interstitial sites. Stability of the α″ martensite phase against the parent β phase is usually evaluated by the axial ratio *b*/*a*, which indicates the progress of the shearing process of the martensitic transformation. For bcc and hcp structures, the *b*/*a* is $\sqrt{2}$ and $\sqrt{3}$, respectively. Thus, the *b*/*a* of α″ martensite changes from $\sqrt{2}$ to $\sqrt{3}$ depending on the stability of the α″ martensite phase. In Ti–Nb binary alloys [2,19–21], the *b*/*a* increases as the Nb content decreases to $\sqrt{3}$ in the Ti-5.7Nb (at.%) alloy [22] and the crystal structure of the α″ martensite changes to hcp (α′ phase). Fig. 2(c) shows the *b*/*a* of 0O, 0.3O, and 0.5O alloys. The *b*/*a* increased with increasing oxygen content; therefore, the α″ martensite phase was stabilized and crystal structure of α″ martensite changed to an hcp-like structure due to the addition of oxygen atoms.

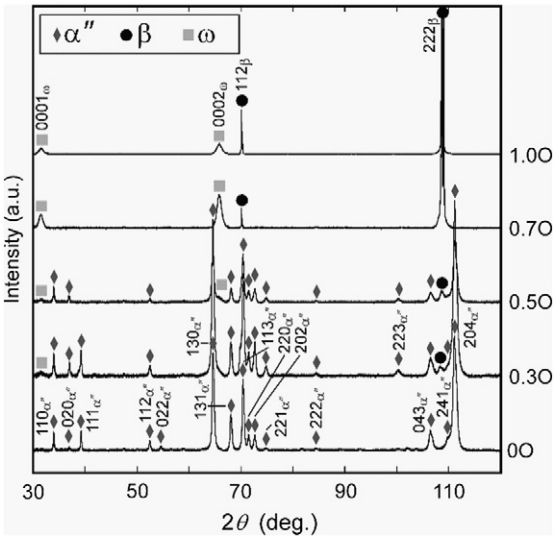


**Fig. 1.** XRD profiles of the 0O, 0.3O, 0.5O, 0.7O, and 1.0O alloys.

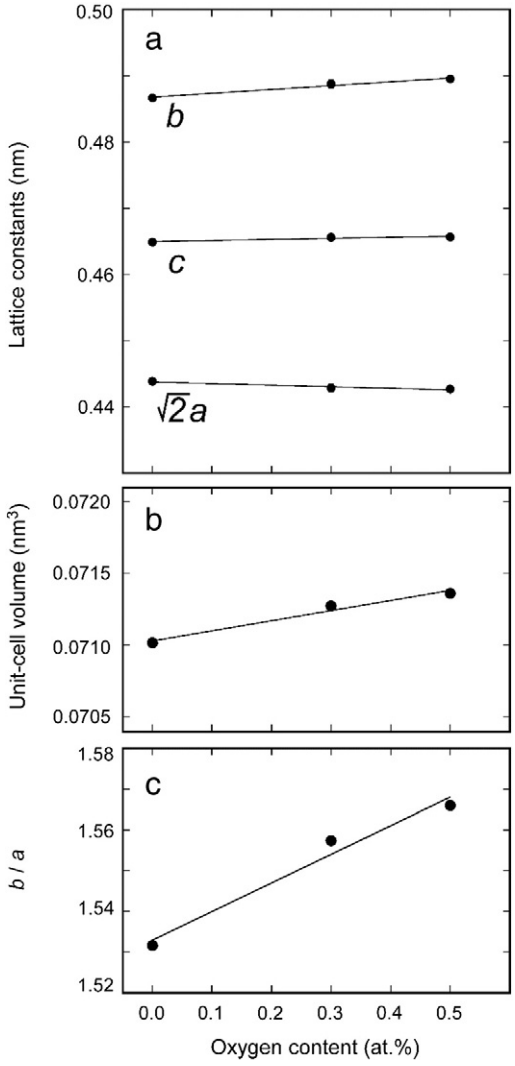


**Fig. 2.** Oxygen content dependence on (a) lattice constants of the α″ martensite phase, (b) unit-cell volume, and (c) axial ratio *b*/*a*.

Changes in the stability of α″ martensite are directly linked to the martensitic transformation temperatures. DSC measurements were carried out for the 0O, 0.3O, and 0.5O alloys, and the curves are shown in Fig. 3. In all alloys, the endothermic peak corresponding to the reverse martensitic transformation from the α″ martensite phase to the parent β phase was observed during heating. In the 0O and 0.3O alloys, a small exothermic peak was observed just after the reverse martensitic transformation as shown in Fig. 3. It has been reported that the appearance of this exothermic peak above the reverse martensitic transformation temperature corresponds to the rapid formation of an isothermal-ω phase in the parent β phase [23]. In the 0.5O alloy, the exothermic peak just after the reverse martensitic transformation, indicating the formation of the isothermal-ω phase, was not observed. This means that the addition of oxygen suppressed the formation of the isothermal-ω phase. A similar result was reported by Williams et al. [24]. The arrows in Fig. 3 indicate the peak temperature of the reverse transformation ($A^*$). $A^*$ increased slightly as the oxygen content increased, and this result also suggests that the α″ martensite was stabilized by the addition of oxygen atoms. This is consistent with the increase of *b*/*a* caused by the addition of oxygen (Fig. 2(b)).

Oxygen addition suppressed the formation of α″ martensite of the Ti-20Nb alloy and α″ martensite was not observed at room temperature

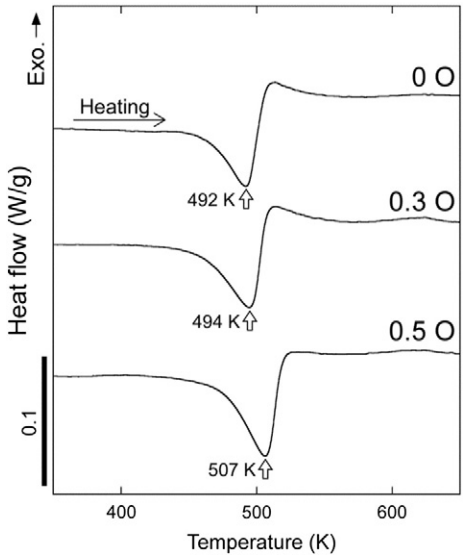


**Fig. 3.** DSC curves of the 0O, 0.3O, and 0.5O alloys.

in the 0.7O and 1.0O alloys, and thus the $M_s$ was decreased by the addition of oxygen (Fig. 4(a)). However, the oxygen atoms in the α″ martensite phase stabilized the α″ martensite (Figs. 2 and 3). Important factors in understanding these observations are the interstitial oxygen atom sites and the directions of the local strain field generated by oxygen atoms in the β and α″ phases. Oxygen atoms in the parent β phase occupy the three types of octahedral sites and they generate local strain fields along $[100]_\beta$, $[010]_\beta$, and $[001]_\beta$. The distribution of these three types of interstitial sites is random and even in the β phase. As shown in Fig. 4(b) [14], the local strain fields along $<100>_\beta$ can be relaxed by shuffling adjacent $\{110\}_\beta$ planes in the $\langle 1\,1\,0\rangle_\beta$ directions (i.e., shuffling process of the β–α″ martensitic transformation), which corresponds to the nanodomains. There are six variants (V1–V6) for the nanodomains, depending on the direction of local strain fields induced by oxygen atoms in the β phase. When the three types of interstitial sites were distributed evenly and randomly in the β phase, all six variants of the nanodomains were induced (Fig. 4(a)). These nanodomains suppressed the formation of long-range α″ martensite; therefore, the β phase was stabilized by oxygen atoms and nanodomains. However, determining the position of oxygen atoms in α″ martensite is extremely difficult, although it is expected that the oxygen atoms in the α″ martensite occupy the two types of octahedral sites (Fig. 4(c)) because the *b*- and *c*-axes increased and the *a*-axis decreased with increasing oxygen content. Oxygen atoms at these two sites generate the local strain fields along $[0, 1/2 + \delta, 1/2]\alpha''$ and $[0, 1/2 + \delta, -1/2]\alpha''$, indicated by black arrows in Fig. 4(c), where $\delta$ is the magnitude of the shuffling displacement of the $\{110\}_\beta$ planes in the β–α″ martensitic transformation. For α″ martensite, $\delta$ changes from 0 (bcc) to 1/6 (hcp) depending on the stability of the α″ martensite phase. Both of the two types of local strain fields introduced by the oxygen atoms in the α″ martensite enhance the shuffling and shearing processes of the β–α″ martensitic transformation, because these processes relax the local strain fields. From the XRD measurements of this study, the changes in the shuffling process ($=\delta$) in the α″ martensite cannot be determined; however, the shearing process ($=b/a$) in α″ martensite progressed with increasing oxygen content, as shown in Fig. 2(c). As a result, oxygen atoms enhanced the shuffling and shearing, transforming the α″ martensite to an hcp-like structure through the addition of oxygen. This is the mechanism by which oxygen atoms stabilize α″ martensite in the α″ phase of the Ti–Nb alloy.

In both the β and α″ phases, the role of interstitial oxygen atoms is similar: oxygen atoms expand the surrounding atoms (Ti and Nb), then generate and promote the shuffling and shearing processes of the β–α″ martensitic transformation. In the parent β phase, all modes of shuffling, namely nanodomains, were induced by the random and even oxygen atom distribution. These nanodomains prevent the formation of long-range α″ martensite, and thus the oxygen atoms in the β phase suppressed the β–α″ martensitic transformation. However, the oxygen atoms in the α″ martensite phase promoted the same mode of shuffling and shearing; therefore, the increase in the axial ratio *b*/*a* increased the stability of the α″ martensite through the addition of oxygen atoms.

In summary, in Ti-20 at.% Nb alloys containing oxygen, the α″ martensite phase was stabilized by the strain fields of oxygen atoms. As the oxygen content increased, the axial ratio *b*/*a* of α″ martensite and the reverse transformation temperature increased. These phenomena were explained by the relaxation of the strain field introduced by oxygen atoms in α″ martensite.

## Acknowledgment

This work was supported by a Grant-in-Aid for Scientific Research (Kiban S 26220907, Wakate B 26870194, Kiban B 15H04143) from the Japan Society for the Promotion of Science and the Advanced Low Carbon Technology Research and Development Program (JY240121) of the Japan Science and Technology Agency.

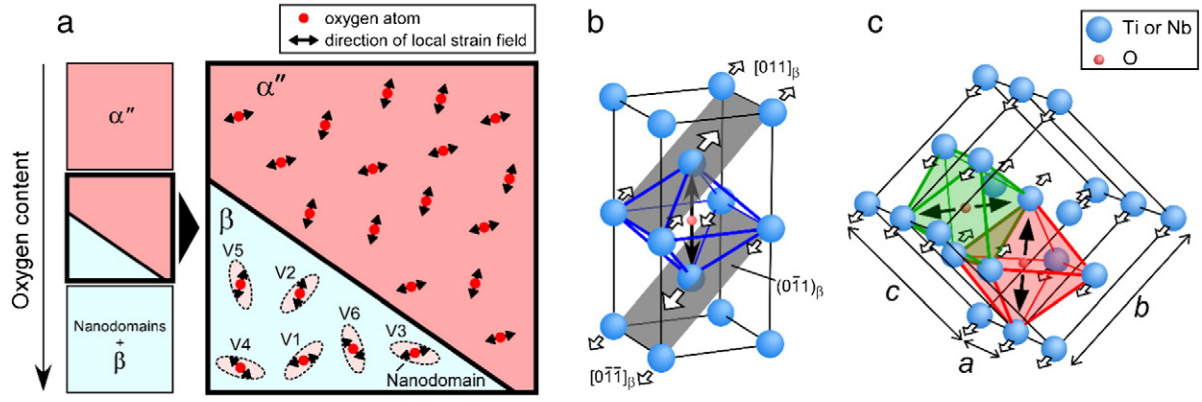


**Fig. 4.** (a) Schematic illustration explaining the effect of oxygen addition on the phase constitution of Ti–Nb alloys. Schematic illustrations of the interstitial oxygen site and relaxation of local strain fields introduced by oxygen atoms in the (b) parent β, and (c) α″ martensite phases.

## References


[1] T.W. Duerig, D.F. Richter, J. Albrecht, Acta Metall. Mater. 30 (1982) 2161–2172.
[2] H.Y. Kim, Y. Ikehara, J.I. Kim, H. Hosoda, S. Miyazaki, Acta Mater. 54 (2006) 2419–2429.
[3] E. Takahashi, T. Sakurai, S. Watanabe, N. Masahashi, S. Hanada, Mater. Trans. 43 (2002) 2978–2983.
[4] J.I. Kim, H.Y. Kim, H. Hosoda, S. Miyazaki, Mater. Trans. 46 (2005) 852–857.
[5] D.H. Ping, Y. Mitarai, F.X. Yin, Scripta Mater. 52 (2005) 1287–1291.
[6] T. Furuhara, S. Annaka, Y. Tomio, T. Maki, Mater. Sci. Eng., A 438–440 (2006) 825–829.
[7] E.G. Obbard, Y.L. Hao, R.J. Talling, S.J. Li, Y.W. Zhang, D. Dye, R. Yang, Acta Mater. 59 (2011) 112–125.
[8] M. Besse, P. Castany, T. Gloriant, Acta Mater. 59 (2011) 5982–5988.
[9] A. Ramarolahy, P. Castany, F. Prima, P. Laheurte, I. Péron, T. Gloriant, J. Mech. Behav. Biomed. Mater. 9 (2012) 83–90.
[10] M. Tahara, H.Y. Kim, H. Hosoda, S. Miyazaki, Funct. Mater. Lett. 2 (2009) 79–82.
[11] M. Tahara, H.Y. Kim, H. Hosoda, T.H. Nam, S. Miyazaki, Mater. Sci. Eng., A 527 (2010) 6844–6852.
[12] C. Hammond, Scr. Metall. Mater. 6 (1972) 569–570.
[13] Y. Nii, T. Arima, H.Y. Kim, S. Miyazaki, Phys. Rev. B 82 (2010) 214104.
[14] M. Tahara, H.Y. Kim, T. Inamura, H. Hosoda, S. Miyazaki, Acta Mater. 59 (2011) 6208–6218.
[15] H.Y. Kim, L. Wei, S. Kobayashi, M. Tahara, S. Miyazaki, Acta Mater. 61 (2013) 4874–4886.
[16] M. Tahara, H.Y. Kim, T. Inamura, H. Hosoda, S. Miyazaki, J. Alloy. Compd. 577 (2013) S404–S407.
[17] M. Tahara, T. Kanaya, H.Y. Kim, T. Inamura, H. Hosoda, S. Miyazaki, Acta Mater. 80 (2014) 317–326.
[18] N.E. Paton, J.C. Williams, Scr. Metall. 7 (1973) 647–649.
[19] A.R.G. Brown, D. Clark, J. Eastabrook, K.S. Jepson, Nature 201 (1964) 914–915.
[20] S. Banumathy, R.K. Mandal, A.K. Singh, J. Appl. Phys. 106 (2009) 093518-093518-093516.
[21] D.L. Moffat, D.C. Larbalestier, Metall. Trans. A 19 (1988) 1677–1686.
[22] E.W. Collings, The Physical Metallurgy of Titanium Alloys, ASM, 1984.
[23] Y. Mantani, M. Tajima, Mater. Sci. Eng., A 438–440 (2006) 315–319.
[24] J.C. Williams, B.S. Hickman, D.H. Leslie, Metall. Trans. 2 (1971) 477–484.